Cell Host & Microbe
Article

A Secreted Bacterial Protease Tailors the *Staphylococcus aureus* Virulence Repertoire to Modulate Bone Remodeling during Osteomyelitis

James E. Cassat,[1] Neal D. Hammer,[2] J. Preston Campbell,[4] Meredith A. Benson,[5] Daniel S. Perrien,[3,6,7] Lara N. Mrak,[8] Mark S. Smeltzer,[8] Victor J. Torres,[5] and Eric P. Skaar[2,*]
[1]Department of Pediatrics, Division of Pediatric Infectious Diseases
[2]Department of Pathology, Microbiology, and Immunology
[3]Department of Orthopaedic Surgery and Rehabilitation
Vanderbilt University School of Medicine, Nashville, TN 37232, USA
[4]Department of Pharmacology, Vanderbilt University, Nashville, TN 37232, USA
[5]Department of Microbiology, New York University Medical Center, New York, NY 10016, USA
[6]Vanderbilt Center for Bone Biology, Vanderbilt University Medical Center, Nashville, TN 37232, USA
[7]Department of Veterans Affairs, Tennessee Valley Healthcare System, Nashville, TN 37212, USA
[8]Department of Microbiology and Immunology, University of Arkansas for Medical Sciences, Little Rock, AR 72205, USA
*Correspondence: eric.skaar@vanderbilt.edu
http://dx.doi.org/10.1016/j.chom.2013.05.003

SUMMARY

Osteomyelitis is a common manifestation of invasive *Staphylococcus aureus* infection. Pathogen-induced bone destruction limits antimicrobial penetration to the infectious focus and compromises treatment of osteomyelitis. To investigate mechanisms of *S. aureus*-induced bone destruction, we developed a murine model of osteomyelitis. Microcomputed tomography of infected femurs revealed that *S. aureus* triggers profound alterations in bone turnover. The bacterial regulatory locus *sae* was found to be critical for osteomyelitis pathogenesis, as Sae-regulated factors promote pathologic bone remodeling and intraosseous bacterial survival. Exoproteome analyses revealed the Sae-regulated protease aureolysin as a major determinant of the *S. aureus* secretome and identified the phenol-soluble modulins as aureolysin-degraded, osteolytic peptides that trigger osteoblast cell death and bone destruction. These studies establish a murine model for pathogen-induced bone remodeling, define Sae as critical for osteomyelitis pathogenesis, and identify protease-dependent exoproteome remodeling as a major determinant of the staphylococcal virulence repertoire.

INTRODUCTION

Osteomyelitis is one of the most common invasive manifestations of *Staphylococcus aureus* infection, and *S. aureus* is the most frequent etiologic agent of musculoskeletal infection (Lew and Waldvogel, 2004). In children, staphylococcal osteomyelitis accounts for approximately 2.5 out of every 1,000 hospital admissions, with annual incidence estimates ranging from 1 in 5,000 to 1 in 10,000 (Gerber et al., 2009; Weichert et al., 2008). Among adults, osteomyelitis frequently complicates such comorbidities as open fractures, contiguous soft-tissue infections, and diabetes (Lew and Waldvogel, 1997). However, in the era of community-acquired methicillin-resistant *S. aureus* (CA-MRSA), osteomyelitis now most frequently occurs in patients who have no appreciable risk factors for invasive staphylococcal infection.

Treatment of osteomyelitis is complex and typically involves one or more surgical debridements followed by prolonged antimicrobial therapy. Even with an appropriate antimicrobial regimen, patients suffering from staphylococcal osteomyelitis frequently experience serious, life-threatening complications such as septicemia, venous thrombosis, and pathologic fractures (Belthur et al., 2012; Gonzalez et al., 2006). Such complications are related to the ability of *S. aureus* to incite significant bone destruction, trigger surrounding soft-tissue inflammation, and ultimately disseminate via the bloodstream. Bone destruction during osteomyelitis also confounds therapy by limiting antimicrobial penetration to the infectious focus. For this reason, prolonged antimicrobial treatment is required for osteomyelitis. An enhanced understanding of the mechanisms that promote bone destruction during osteomyelitis could facilitate development of therapies that limit bone destruction, thus improving the efficacy of current antimicrobials while reducing adverse outcomes. However, little is known regarding the specific bacterial factors that promote bone destruction during osteomyelitis.

Previous in vitro studies have investigated the interaction between *S. aureus* and the cells responsible for bone remodeling, osteoblasts and osteoclasts. *S. aureus* is capable of invading and persisting within osteoblasts (Ellington et al., 1999; Hudson et al., 1995). The interaction of *S. aureus* and osteoblasts leads to physiologic alterations that favor bone resorption by two primary mechanisms. First, *S. aureus*-infected osteoblasts incite osteoclastogenesis through increased expression of proinflammatory cytokines and the critical osteoclast-activating molecule receptor activator of NF-κB ligand (RANK-L) (Claro et al., 2013; Marriott et al., 2004; Somayaji et al., 2008). Second, *S. aureus* invasion of osteoblasts results

in cell death (Alexander et al., 2003; Young et al., 2011). However, the specific staphylococcal factors that trigger osteoblast cell death or induce osteoclastogenesis are unknown. Furthermore, it has yet to be determined whether these in vitro phenomena are responsible for pathogen-mediated bone destruction in vivo.

In this manuscript, a murine model of osteomyelitis is established to investigate staphylococcal factors contributing to the pathogenesis of osteomyelitis. Through the use of high-resolution microcomputed tomography (microCT), global proteomic analyses, and cell culture assays, specific staphylococcal virulence factors that contribute to pathologic bone remodeling and intraosseous bacterial survival are identified. Additionally, a significant role is identified for the secreted protease aureolysin in shaping the staphylococcal virulence repertoire during invasive infection. The tools developed in this work are readily adaptable to a variety of bacterial species, allowing for detailed analyses of the interaction between bacterial pathogens and bone.

RESULTS

Establishment of a Murine Model of Osteomyelitis for the Study of Pathologic Bone Remodeling and Intraosseous Bacterial Survival

For interrogation of the mechanisms of pathologic bone remodeling and intraosseous bacterial survival during osteomyelitis, a murine model was created. Derivatives of the USA300 type strain LAC were used as the wild-type (WT) for all infections, as USA300 type clinical isolates are common causes of musculoskeletal infections in both adults and children (Carrillo-Marquez et al., 2009; Peyrani et al., 2012). For induction of osteomyelitis, 1×10^6 colony-forming units (cfu) of *S. aureus* are inoculated into the intramedullary canal of murine femurs after the creation of a 1 mm unicortical bone defect. Infected femurs exhibit peak bacterial burdens by day 4 postinfection (data not shown) and display profound changes in bone remodeling surrounding the inoculation site by day 14 postinfection. In addition to progressive cortical bone destruction at the inoculation site, infected femurs display marked new bone formation peripheral to the infectious focus (Figure 1A). In contrast, mice mock infected with sterile PBS experience healing of the surgically induced cortical bone defect by day 14 postinfection (Figure 1B). For quantification of both cortical bone destruction and peripheral new bone formation, imaging analysis algorithms were created and applied to images of both infected and mock-infected femurs. Infected femurs sustain significantly more cortical bone destruction and peripheral new bone formation than do mock-infected femurs (Figure 1C and 1D). Quantitative imaging analyses underscored the magnitude of changes in bone remodeling during osteomyelitis, as infected femurs lost approximately 10%–20% of total cortical volume near the infectious focus, while peripheral new bone formation accounted for bone growth of approximately 30%–50% of the entire original cortical volume (data not shown). Histopathologic examination confirmed microCT findings, while also demonstrating substantial abscess formation throughout the bone marrow of infected femurs (Figure 1E). In contrast, the bone marrow architecture of mock-infected femurs remains intact (Figure 1F). Collectively, these results establish a murine model of staphylococcal osteomyelitis amenable to imaging analysis of pathologic bone remodeling and demonstrate that *S. aureus* infection incites profound changes in bone turnover.

S. aureus-Secreted Virulence Factors Contribute to the Pathogenesis of Osteomyelitis

Based on the distinct zones of cortical bone destruction and peripheral new bone formation surrounding the inoculation site in infected murine femurs, we hypothesized that secreted staphylococcal factors trigger concentration-dependent changes in bone remodeling and enhance bacterial survival in the bone. So that this hypothesis could be tested, mice were infected with a *S. aureus* strain rendered exoprotein-deficient by virtue of mutations in the global regulatory loci *agr* and *sae* (Δ*agr/sae*). SDS-PAGE analysis of concentrated culture supernatants confirmed that in comparison to the WT, Δ*agr/sae* has a severely limited exoprotein profile, with inactivation of either *agr* (Δ*agr*) or *sae* (Δ*sae*) alone having more modest effects (Figure S1 available online). For investigation of the contribution of the *agr* and *sae* loci to the pathogenesis of *S. aureus* osteomyelitis, groups of mice were infected with either WT or Δ*agr/sae*. At 14 days postinfection, infected femurs were harvested and either subjected to microCT imaging or processed to quantify bacterial burdens. Femurs infected with Δ*agr/sae* have significantly less cortical bone destruction and peripheral new bone formation when compared to the WT (Figures 2A–2D). Additionally, femurs infected with Δ*agr/sae* have significantly lower bacterial burdens than WT-infected femurs (Figure 2E). Together, these results reveal that the *agr* and *sae* regulatory loci are critical to the pathogenesis of *S. aureus* osteomyelitis and suggest that Agr- or Sae-regulated virulence factors contribute to pathologic bone remodeling and intraosseous bacterial survival.

The *sae* Regulatory Locus Contributes to Pathologic Bone Remodeling and Intraosseous Bacterial Survival during *S. aureus* Osteomyelitis

For further delineation of specific *S. aureus* virulence factors that contribute to pathologic bone remodeling and intraosseous bacterial survival during osteomyelitis, mice were infected with strains inactivated for either *agr* (Δ*agr*) or *sae* (Δ*sae*) and compared to WT-infected mice. At 14 days postinfection, femurs were harvested and subjected to microCT imaging or processed to quantify bacterial burdens. Murine femurs infected with Δ*sae* sustain significantly less cortical bone destruction and new bone formation than WT-infected femurs (Figures 3A–3F). Moreover, Δ*sae*-infected femurs have a significant decrease in bacterial burdens when compared to WT-infected femurs, showing a similar reduction to that observed in Δ*agr/sae*-infected femurs (Figure 3G). Conversely, murine femurs infected with Δ*agr* exhibit no significant change in bacterial burdens relative to WT-infected femurs, but sustain significantly less cortical bone destruction (Figure S2). Collectively, these studies define the *sae* and *agr* regulatory loci as contributors to pathologic bone remodeling during *S. aureus* osteomyelitis, with *sae* also significantly impacting intraosseous bacterial survival.

Sae-Regulated Secreted Virulence Factors Are Cytotoxic to Osteoblasts

In vivo studies revealed a critical role for the *sae* regulatory locus in the pathogenesis of *S. aureus* osteomyelitis. In order to

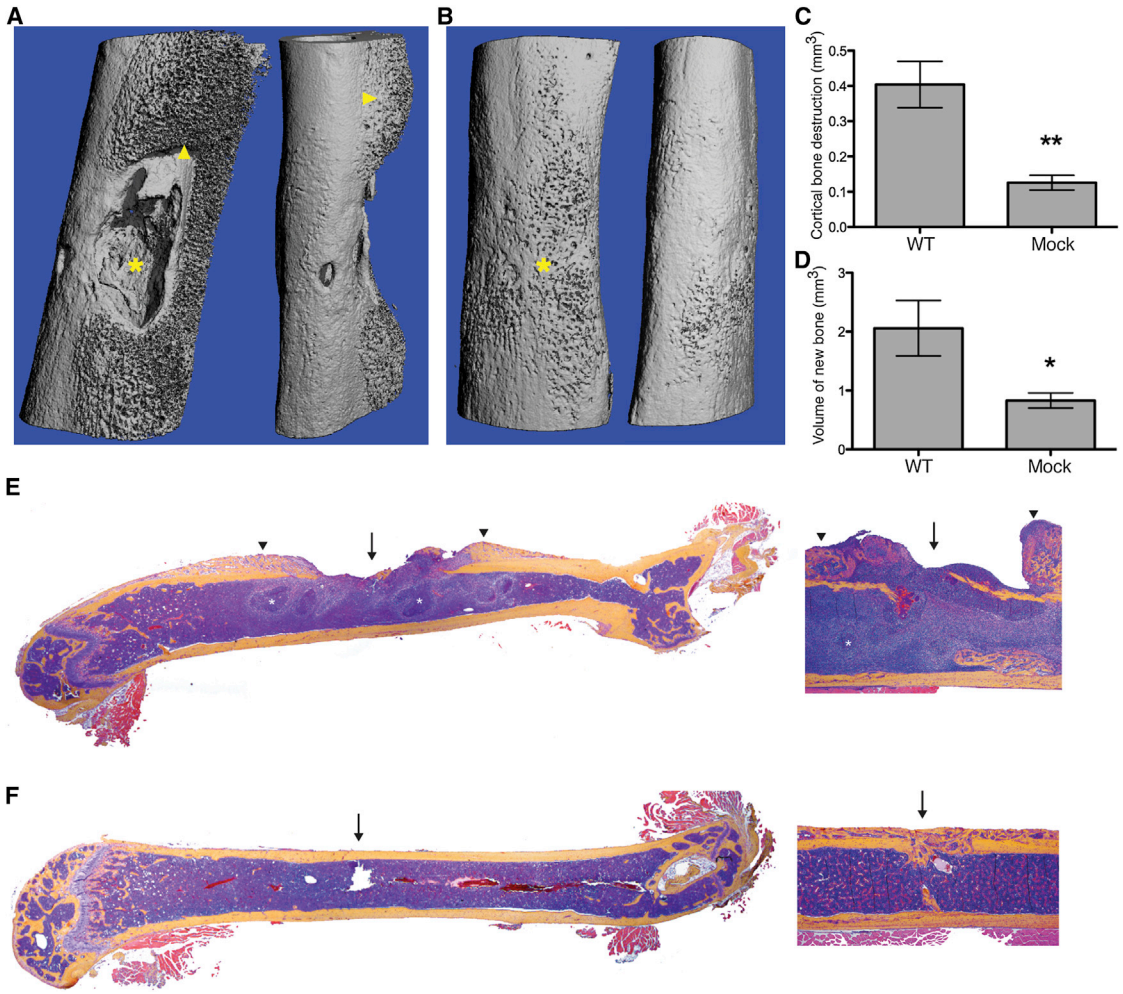

Figure 1. *S. aureus* Triggers Pathologic Bone Remodeling during Osteomyelitis

Groups of mice were subjected to experimental osteomyelitis via intramedullary inoculation of either *S. aureus* strain LAC (WT) or an equivalent volume of sterile PBS (mock). Femurs were harvested at 14 days postinoculation and subjected to microCT analysis.

(A) Anteroposterior (left) and lateral (right) views of a *S. aureus*-infected femur at 14 days postinoculation. Asterisk denotes inoculation site and surrounding cortical bone destruction. Arrowheads denote peripheral new bone formation.

(B) Anteroposterior (left) and lateral (right) views of a mock-infected femur at 14 days postinoculation. Asterisk denotes inoculation site.

(C and D) MicroCT imaging analysis of cortical bone destruction (C) and new bone formation (D) in infected femurs at day 14 postinoculation. n = 4 mice per group. Error bars indicate the SEM. *$p < 0.05$ and **$p < 0.01$ relative to WT infection as calculated by a Student's t test.

(E and F) Modified hematoxylin and eosin (H&E)-phloxine-orange-G-stained sections of representative WT-infected (E) or mock-infected (F) femurs at low (left) or high (right) magnification. High-magnification images are centered over the inoculation site and represent different tissue depths from the same femurs in low-magnification images. Arrows denote inoculation site, arrowheads denote peripheral new bone formation, and asterisks denote abscesses.

investigate the mechanism by which Sae-regulated virulence factors perturb bone remodeling, a cytotoxicity assay was developed with murine (MC3T3) and human (Saos-2) osteoblastic cells. Incubation of MC3T3 or Saos-2 cell monolayers with concentrated culture supernatant from WT *S. aureus* results in potent cytotoxicity (Figures 4A and 4B). Cytotoxicity is observed as early as 2 hr after the addition of culture supernatant (data not shown). Incubation of MC3T3 cell monolayers with varying amounts of unconcentrated culture supernatant revealed that cytotoxicity is dose dependent (Figure 4C). Inactivation of the *sae* locus leads to a complete loss of cytotoxicity in both murine and human osteoblastic cells after intoxication with concentrated supernatant (Figures 4A and 4B). However, when osteoblast monolayers are incubated with unconcentrated culture supernatant from Δ*sae*, a significant increase in cytotoxicity relative to concentrated supernatant preparations is observed (Figure 4A). Importantly, the enhanced cytotoxicity of unconcentrated Δ*sae* supernatant was not explained simply by differences in protein abundance in the concentrated versus unconcentrated samples, as roughly equivalent final protein concentrations were added to cell monolayers (data not shown). Rather, as supernatant concentration required an additional 3 hr of sample processing, an alternative explanation is that loss of cytotoxicity in Δ*sae* concentrated culture supernatant is due to increased degradation of osteolytic factors over time. Together, these results reveal that secreted *S. aureus* factors

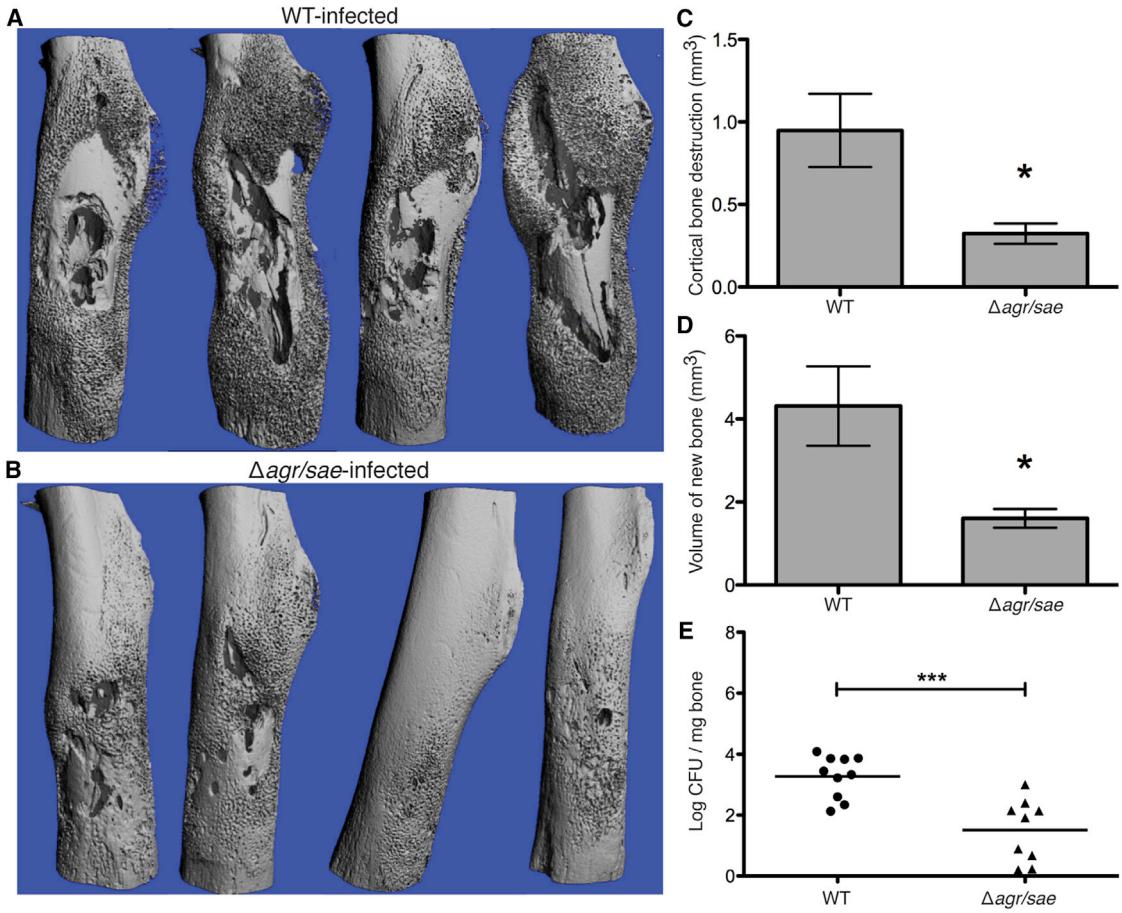

Figure 2. *S. aureus*-Secreted Virulence Factors Contribute to Pathologic Bone Remodeling and Intraosseous Bacterial Survival during Osteomyelitis

Groups of mice were subjected to experimental osteomyelitis via inoculation of WT or Δ*agr/sae*. Femurs were harvested at 14 days postinoculation and subjected to microCT imaging analysis or processed for enumeration of bacterial burdens.

(A and B) Anteroposterior views of WT- (A) or Δ*agr/sae*- (B) infected femurs at 14 days postinoculation.

(C and D) MicroCT imaging analysis of cortical bone destruction (C) and new bone formation (D) in infected femurs at day 14 postinoculation. n = 4 mice per group. Error bars indicate the SEM. *$p < 0.05$ relative to the WT as calculated by a Student's t test.

(E) Colony-forming unit (cfu) recovery per milligram of bone tissue at day 14 postinoculation. n = 9 (Δ*agr/sae*) or n = 10 (WT) per group. ***$p < 0.001$ as calculated by a Student's t test. Horizontal bars represent the mean of log cfu/mg of bone.

See also Figure S1.

are dose-dependently cytotoxic to both human and murine osteoblastic cells and suggest that these osteolytic factors experience enhanced degradation in the absence of Sae.

Analysis of the Sae Exoproteome Identifies Aureolysin as a Significant Determinant of the *S. aureus*-Secreted Virulence Repertoire

Osteoblast cytotoxicity assays suggested that *S. aureus* secretes osteolytic factors that experience enhanced degradation in the absence of Sae. For identification of Sae-regulated exoproteins that elicit osteoblast cell death and contribute to the pathogenesis of *S. aureus* osteomyelitis, the Sae exoproteome was determined. Multidimensional protein identification technology (MudPIT) analyses were performed on concentrated culture supernatants from WT and Δ*sae*. Spectral counts were determined and used as a measure of protein abundance. Inactivation of *sae* leads to a significant decrease in the abundance of 49 proteins, including secreted virulence factors such as cytotoxins (Hla, LukA, LukB, HlgA, HlgC, and PVL), immunomodulatory molecules (CHIPS, Sbi, and Fprl1 inhibitory protein), and exoenzymes (SplA-F and Nuc) (Table 1). A file containing all proteins that change in abundance upon inactivation of *sae* is also included in the Supplemental Information (Table S1). Thirty-one proteins significantly increase in abundance upon inactivation of *sae*, and of these, the secreted protease aureolysin is most altered, increasing 8-fold (Table 1 and Table S1). Based on the observation that inactivation of *sae* leads to decreased abundance of osteolytic factors (Figure 4A) and globally altered exoprotein patterns (Figure S1), we hypothesized that aureolysin activity might significantly modify the Sae exoproteome. Therefore, the exoproteome of a strain inactivated for both *sae* and *aur* (Δ*sae/aur*) was determined. Concomitant inactivation of *sae* and *aur* leads to profound changes in the exoproteome, with 230 proteins significantly increasing in abundance and 51

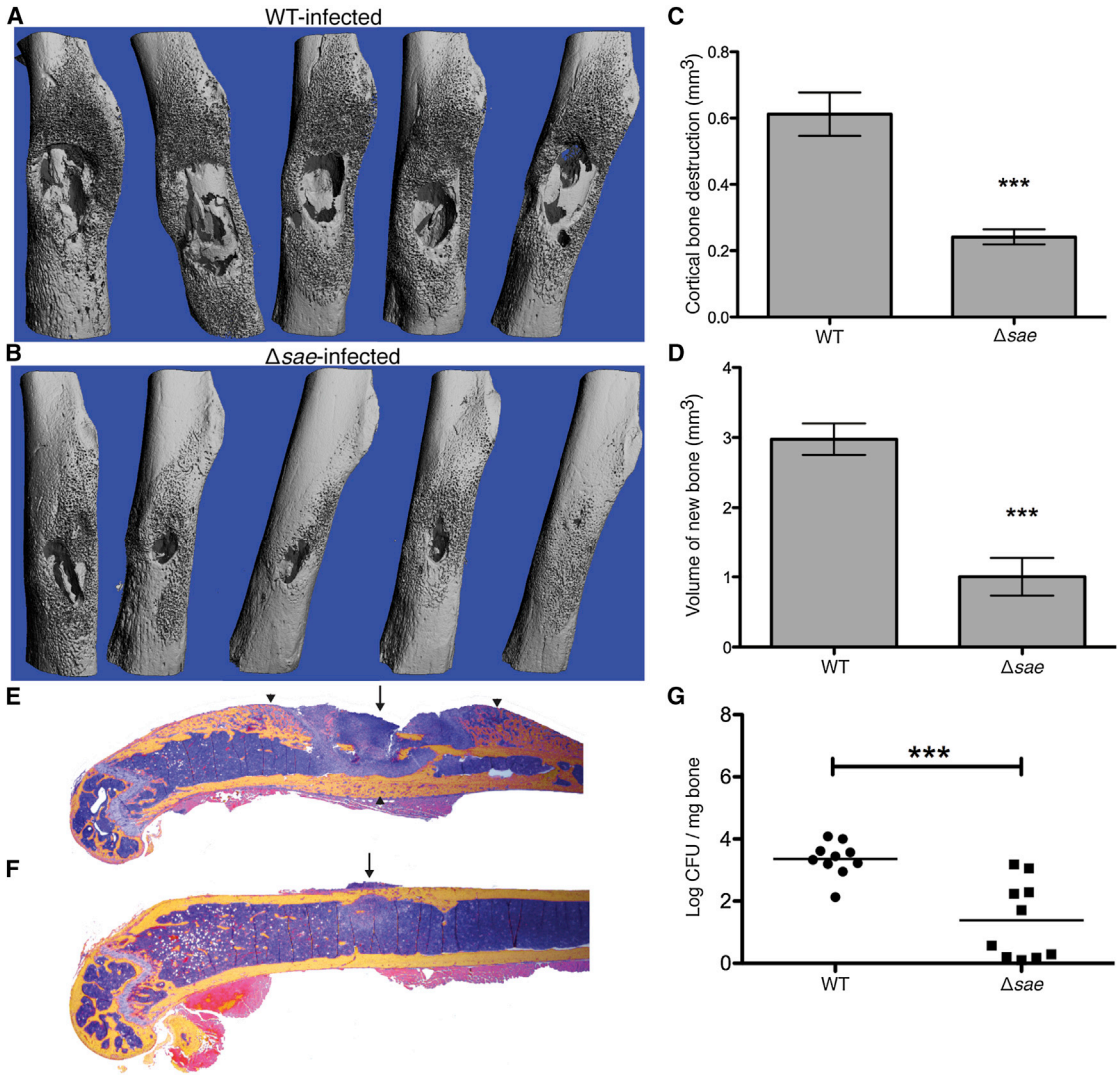

Figure 3. The *sae* Regulatory Locus Contributes to Pathologic Bone Remodeling and Intraosseous Bacterial Survival during *S. aureus* Osteomyelitis

Groups of mice were subjected to experimental osteomyelitis via inoculation of WT or Δ*sae*. Femurs were harvested at 14 days postinoculation and subjected to microCT imaging analysis or processed for enumeration of bacterial burdens.

(A and B) Anteroposterior views of WT- (A) or Δ*sae*- (B) infected femurs at 14 days postinoculation.

(C and D) MicroCT imaging analysis of cortical bone destruction (C) and new bone formation (D) in infected femurs at day 14 postinoculation. n = 5 mice per group. Error bars indicate the SEM. ***p < 0.001 relative to the WT as calculated by a Student's t test.

(E and F) Modified H&E-phloxine-orange-G-stained sections of representative WT-infected (E) or Δ*sae*-infected (F) femurs at low magnification. Arrows denote inoculation site, and arrowheads denote peripheral new bone formation.

(G) Colony-forming unit (cfu) recovery per milligram of bone tissue at day 14 postinoculation. n = 10 per group. ***p < 0.001 as calculated by a Student's t test. Horizontal bars represent the mean of log cfu/mg of bone.

See also Figure S2.

proteins significantly decreasing in abundance relative to the WT (Table 2 and Table S2). Of the 269 proteins that decrease in abundance upon inactivation of *sae*, 225 (83%) increase in abundance upon concomitant inactivation of *aur*, with 190 (84%) of these proteins either returning to or exceeding WT protein levels (Table S2). Thus, the Sae exoproteome is significantly impacted by the activity of aureolysin, with the majority of Sae-regulated exoproteins experiencing aureolysin-dependent changes in abundance. These findings support a model whereby the Sae-regulated protease aureolysin remodels the staphylococcal exoproteome to modulate virulence.

Inactivation of Aureolysin in the Δ*sae* Background Restores Osteoblast Cytotoxicity and Increases Cortical Bone Destruction

Exoproteome analyses revealed that the majority of proteins that decrease in abundance upon inactivation of *sae* do so in an aureolysin-dependent manner. We therefore hypothesized that

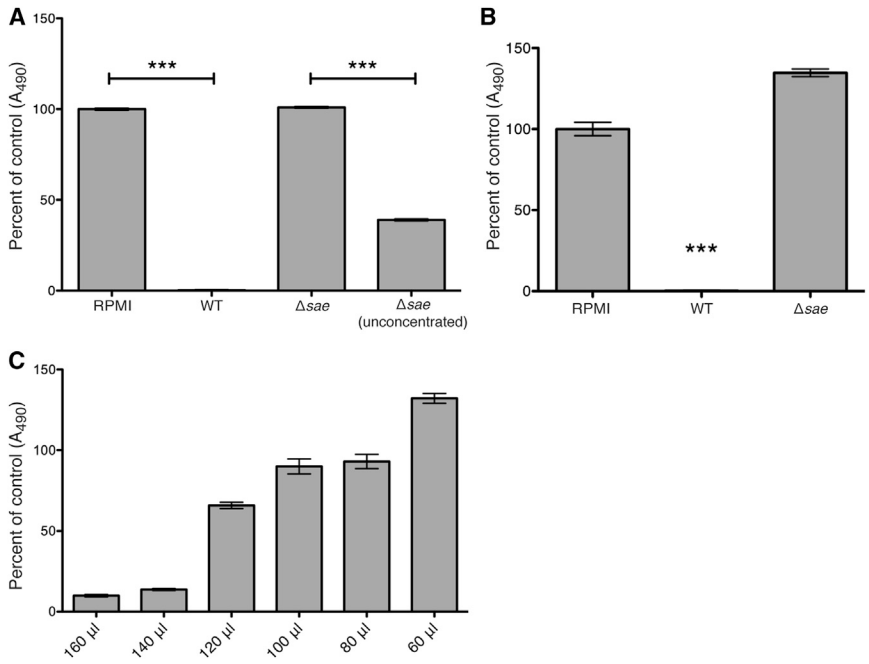

Figure 4. Sae-Regulated Secreted Virulence Factors Are Dose-Dependently Cytotoxic to Osteoblasts

(A and B) MC3T3 murine osteoblastic cells (A) or Saos-2 human osteoblastic cells (B) were seeded into 96-well plates at 5,000 cells per well or 10,000 cells per well, respectively. After 24 hr, growth media were replaced, and 40 μl concentrated culture supernatant, 160 μl unconcentrated supernatant, or an equivalent volume of sterile RPMI supplemented with 1% casamino acids (control) was added to cell monolayers. Osteoblast viability was assessed 23 hr later with the Promega CellTiter 96 AQueous One kit, and results are expressed as percent of control. n = 10 per group and results are representative of at least three independent experiments. Error bars indicate the SEM. ***$p < 0.001$ as calculated by a Student's t test.

(C) MC3T3 cells were seeded into 96-well plates at a density of 2,500 cells per well. Twenty-four hours after seeding, growth media were replaced and varying amounts of unconcentrated culture supernatant were added to cell monolayers. Cell viability was assessed as above. n = 10 per group. Error bars indicate the SEM.

the lack of osteoblast cytotoxicity in concentrated supernatant preparations from Δ*sae* was due to aureolysin-mediated degradation of osteolytic exoproteins. So that this hypothesis could be tested, concentrated culture supernatants were prepared from Δ*sae* and Δ*sae/aur*, and each preparation was tested for the ability to induce cell death in murine or human osteoblasts. Inactivation of *aur* in the Δ*sae* background restores cytotoxicity to levels equivalent to the WT in both murine (Figure 5A) and human (data not shown) osteoblasts. For investigation of whether the increased osteoblast cytotoxicity observed with Δ*sae/aur* correlates to increased bone destruction during osteomyelitis, groups of mice were infected with WT, Δ*sae*, or Δ*sae/aur*. At 14 days postinfection, femurs were harvested and imaged by microCT or processed to quantify bacterial burdens. Concomitant inactivation of *aur* does not lead to a significant increase in bacterial recovery from infected femurs relative to inactivation of *sae* alone (Figure 5B). Despite this, inactivation of *aur* in the Δ*sae* background leads to a significant increase in cortical bone destruction (Figure 5C). Taken together, these results demonstrate that inactivation of Sae causes increased abundance of aureolysin, which decreases levels of osteolytic factors and thereby significantly reduces cortical bone destruction. Thus, modulation of the *S. aureus* virulence repertoire by a secreted protease impacts pathogenesis.

Alpha-Type Phenol-Soluble Modulins Are Cytotoxic to Murine and Human Osteoblastic Cells and Contribute to Pathogen-Induced Bone Destruction during Osteomyelitis

Exoproteome analyses revealed proteins with altered abundance upon inactivation of *sae* or concomitant inactivation of *sae* and *aur*. As cytotoxicity was observed with concentrated supernatants from WT and Δ*sae/aur*, but not Δ*sae*, the exoproteomes were analyzed to identify proteins that were detected only in cytotoxic supernatant preparations. The alpha-type phenol-soluble modulins (PSMs) PSMα1 and PSMα2 were present only in the exoproteomes of WT and Δ*sae/aur*, but not in the exoproteome of Δ*sae* (Table S2). Similarly, PSMα4 is present at lower levels in the exoproteome of Δ*sae* as compared to WT and Δ*sae/aur*. The alpha-type PSMs are cytolytic peptides that lyse neutrophils, provoke chemotaxis, and contribute to CA-MRSA virulence (Wang et al., 2007). Additionally, alpha-type PSMs undergo processing by secreted proteases, including aureolysin (Gonzalez et al., 2012; Zielinska et al., 2011). However, the role of PSMs in the pathogenesis of osteomyelitis has not been previously investigated. For testing of the hypothesis that alpha-type PSMs are responsible for osteoblast cytotoxicity, genes encoding the alpha-type PSMs were inactivated in the WT background and concentrated culture supernatant was prepared from this strain. Inactivation of the alpha-type PSMs (Δ*psmα1-4*) leads to a complete loss of cytotoxicity toward both murine and human osteoblastic cells (Figures 5D and 5E), indicating that these peptides are responsible for the cytotoxicity observed with concentrated culture supernatant from WT *S. aureus*. For direct testing of the ability of PSMs to trigger osteoblast cell death, PSMα1, PSMα2, PSMα3, and PSMα4 were synthesized and added directly to MC3T3 or Saos-2 monolayers. PSMα1, PSMα2, and PSMα3 are each dose-dependently cytotoxic to murine and human osteoblasts, with PSMα2 being the most potent (Figures S3A and 3B). In contrast, PSMα4 does not elicit cytotoxicity at concentrations up to 100 μg/ml. For investigation of the impact of aureolysin-mediated processing of PSMs on osteoblast cytotoxicity, PSMα2 and PSMα3 were incubated with purified aureolysin prior to intoxication of MC3T3 monolayers. We were unable to test the effect of aureolysin processing on PSMα1-mediated cytotoxicity due to loss of activity of this peptide after incubation at 37°C (data not shown). Pretreatment of PSMα2 and PSMα3 with aureolysin, but not heat-inactivated aureolysin or buffer control, significantly limits osteoblast cytotoxicity (Figure S3C). So that the contribution of

Table 1. Select Proteins Altered in Abundance upon Inactivation of *sae*

Protein[a]	Mean LAC Spectra	Mean LAC*Δsae* Spectra	LAC/LAC*Δsae*[b]	Description	Quasi p Value[c]
Significantly Decreased: Toxins, Proteases, and Exoenzymes					
Q2FHS2|Q2FHS2_STAA3	242.3333	0.6667	363.5000	Alpha-hemolysin; SAUSA300_1058	0.0014
Q2FFA2|LUKL2_STAA3	157.6667	1.0000	157.6667	LukB; SAUSA300_1975	0.0270
Q2FFA3|LUKL1_STAA3	152.6667	0.0000	152.6667	LukA; SAUSA300_1974	0.0117
Q2FE78|Q2FE78_STAA3	53.6667	0.6667	80.5000	Gamma-hemolysin component A; HlgA	0.0100
Q2FFT1|SPLC_STAA3	24.3333	0.6667	36.5000	Serine protease SplC	0.0242
Q2FJP4|Q2FJP4_STAA3	58.6667	1.6667	35.2000	Putative staphylococcal enterotoxin; SAUSA300_0370	0.0080
Q2FJV7|Q2FJV7_STAA3	67.0000	2.0000	33.5000	5′-nucleotidase, lipoprotein e(P4) family; SAUSA300_0307	0.0024
Q2FFS9|SPLA_STAA3	57.6667	2.6667	21.6250	Serine protease SplA	0.0272
Q2FFT2|SPLD_STAA3	71.0000	5.3333	13.3125	Serine protease SplD	0.0203
Q2FE77|Q2FE77_STAA3	19.0000	1.6667	11.4000	Gamma-hemolysin component C; HlgC	0.0150
Q2FFT0|SPLB_STAA3	261.6667	24.0000	10.9028	Serine protease SplB	0.0150
Q2FGV0|Q2FGV0_STAA3	600.0000	58.0000	10.3448	Panton-Valentine leukocidin, LukF-PV	0.0150
Q2FI16|Q2FI16_STAA3	6.6667	0.6667	10.0000	Chitinase-related protein; SAUSA300_0964	0.0427
Q2FFT4|SPLF_STAA3	75.3333	8.0000	9.4167	Serine protease SplF	0.0217
Q2FJL6|Q2FJL6_STAA3	6.0000	0.6667	9.0000	Exotoxin; SAUSA300_0398	0.0399
Q2FFR8|Q2FFR8_STAA3	26.6667	3.3333	8.0000	Leukotoxin LukE	0.0178
Q2FFT3|SPLE_STAA3	93.6667	12.6667	7.3947	Serine protease SplE	0.0279
Q2FIK2|Q2FIK2_STAA3	216.6667	30.0000	7.2222	Thermonuclease; Nuc	0.0148
Q2FGU9|Q2FGU9_STAA3	191.0000	61.0000	3.1311	Panton-Valentine leukocidin, LukS-PV	0.0446
Significantly Decreased: Immunomodulatory					
Q2FE79|SBI_STAA3	85.6667	0.3333	257.0000	Immunoglobulin-binding protein Sbi	0.0153
Q2FFF7|CHIPS_STAA3	856.0000	7.6667	111.6522	Chemotaxis inhibitory protein; Chp	0.0034
Q2FHS7|FLIPR_STAA3	10.0000	0.0000	10.0000	FPRL1 inhibitory protein; Flr	0.0150
Significantly Decreased: Regulatory					
Q2FIT2|Q2FIT2_STAA3	235.3333	0.0000	235.3333	SaeP; SAUSA300_0693	0.0016
Significantly Decreased: Surface/Cell-Wall Associated					
Q2FE03|FNBA_STAA3	19.3333	0.3333	58.0000	Fibronectin-binding protein A; FnbA	0.0272
Q2FJK6|Q2FJK6_STAA3	30.3333	0.6667	45.5000	Putative surface protein; SAUSA300_0408	0.0063
Q2FHS5|Q2FHS5_STAA3	31.3333	0.0000	31.3333	Fibrinogen-binding protein; Efb; SAUSA300_1055	0.0014
Q2FKM6|Q2FKM6_STAA3	49.6667	2.6667	18.6250	Penicillin-binding protein 2′; MecA	0.0150
Q2FHS4|Q2FHS4_STAA3	6.0000	0.0000	6.0000	Fibrinogen-binding protein; SAUSA300_1056	0.0150
Q2FHU9|Q2FHU9_STAA3	5.3333	1.6667	3.2000	IsdD; SAUSA300_1031	0.0469
Q2FF92|Q2FF92_STAA3	2.0000	0.0000	2.0000	Serine-aspartate repeat family protein, SdrH	0.0024
Significantly Increased: Toxins, Proteases, and Exoenzymes					
Q2FDM2|Q2FDM2_STAA3	16.3333	134.0000	0.1219	Zinc metalloproteinase aureolysin; Aur	0.0080
Q2FKG2|Q2FKG2_STAA3	114.0000	399.3333	0.2854	1-phosphatidylinositol phosphodiesterase; Plc	0.0080
Q2FI30|Q2FI30_STAA3	50.3333	117.3333	0.4290	Cysteine protease; SspB	0.0379
Q2FFI6|Q2FFI6_STAA3	439.0000	885.6667	0.4957	Staphopain A; SAUSA300_1890	0.0178
Q2FIH7|Q2FIH7_STAA3	44.3333	79.0000	0.5612	Staphylococcal enterotoxin Q; Seq	0.0384
Q2FIH8|Q2FIH8_STAA3	27.6667	39.6667	0.6975	Staphylococcal enterotoxin K; Sek	0.0069
Significantly Increased: Regulatory					
Q2FFR1|TRAP_STAA3	5.6667	18.3333	0.3091	Signal transduction protein TRAP	0.0251
Q2FHI3|CODY_STAA3	15.0000	35.3333	0.4245	GTP-sensing transcriptional pleiotropic repressor CodY	0.0279
Significantly Increased: Surface/Cell-Wall Associated					
Q2FHV2|ISDB_STAA3	36.6667	46.0000	0.7971	Iron-regulated surface determinant protein B; IsdB	0.0255
Q2FJ78|SDRD_STAA3	4.3333	19.0000	0.2281	Serine-aspartate repeat-containing protein D; SdrD	0.0081
Q2FDM9|Q2FDM9_STAA3	2.0000	6.6667	0.2999	Clumping factor B; ClfB	0.0272

(*Continued on next page*)

Table 1. ***Continued***

Protein[a]	Mean LAC Spectra	Mean LAC*Δsae* Spectra	LAC/LAC*Δsae*[b]	Description	Quasi p Value[c]
Q2FJ77|SDRE_STAA3	4.0000	10.3333	0.3871	Serine-aspartate repeat-containing protein E; SdrE	0.0247
Q2FE08|Q2FE08_STAA3	57.0000	88.3333	0.6453	Putative cell-wall surface anchor family protein; SAUSA300_2436	0.0489

See also Table S1 for a complete list of proteins that change in abundance upon inactivation of *sae*.
[a]UniprotKB nomenclature (http://www.uniprot.org).
[b]Ratio of mean LAC spectra divided by mean LAC*Δsae* spectra. If mean spectra equaled zero, a value of one was used to calculate ratio. Values greater than 1.0 indicate protein abundances decreased upon inactivation of *sae*. Values less than 1.0 indicate protein abundances increased upon inactivation of *sae*.
[c]False-discovery-rate-corrected p value as calculated by the QuasiTel program.

alpha-type PSMs to pathogen-induced bone destruction during osteomyelitis could be tested, groups of mice were infected with WT or Δ*psmα1-4*, and femurs were harvested for microCT analysis on day 14 postinfection. Inactivation of *psmα1-4* significantly limits cortical bone destruction in infected femurs (30% decrease in cortical bone destruction, p = 0.0156 relative to the WT), demonstrating that osteoblast cytotoxicity induced by the alpha-type PSMs correlates to increased pathogen-induced bone destruction during osteomyelitis (Figure 5F). Collectively, these data identify the alpha-type PSMs as Sae-regulated osteolytic exoproteins that are targeted by aureolysin and contribute to the morbidity of osteomyelitis. These findings confirm that protease-mediated exoproteome remodeling impacts *S. aureus* pathogenesis during invasive infection.

DISCUSSION

Osteomyelitis is a common and debilitating manifestation of invasive *S. aureus* disease. Treatment of osteomyelitis is compromised by pathogen-induced bone destruction, which destroys the vascular architecture of infected bone and limits antimicrobial penetration to the infectious focus. Therapies aimed at limiting bone destruction during osteomyelitis could enhance traditional antimicrobial therapy, while reducing pathologic sequelae. For investigation of the mechanisms by which bacterial pathogens induce bone destruction during osteomyelitis, a murine model of bone infection was developed, and microCT analyses of infected femurs were used to quantify pathologic bone remodeling. These tools revealed that *S. aureus* induces profound changes in bone remodeling, in part through the production of osteolytic exoproteins that modulate osteoblast proliferation. Surprisingly, *S. aureus* infection also leads to profound new bone formation, suggesting that bacterial modulation of bone remodeling involves complex changes in bone physiology. A crucial role for the *S. aureus* regulatory locus *sae* is demonstrated for both pathologic bone remodeling and intraosseous bacterial survival. The animal model of osteomyelitis described here demonstrates quantifiable differences in intraosseous bacterial survival and pathologic bone remodeling between isogenic bacterial strains, making it a valuable tool both for study of osteomyelitis pathogenesis and for the development of new therapies. Furthermore, the surgical techniques and ancillary studies associated with this animal model are easily adaptable to other bacterial species, enabling detailed study of host-pathogen interactions using a variety of bone pathogens. By modeling the interaction between bacterial pathogens and host cells comprising the skeletal system, these tools provide the opportunity to discover the mechanisms underlying bone turnover in response to infectious and inflammatory stimuli.

For identification of osteolytic exoproteins that contribute to pathologic bone remodeling during osteomyelitis, global exoproteome analyses were performed. Exoproteome analysis revealed a crucial role for Sae in the expression of multiple classes of virulence factors, consistent with previous reports that Sae is required for virulence in other animal models of staphylococcal infection (Goerke et al., 2005; Liang et al., 2006; Nygaard et al., 2010; Voyich et al., 2009; Xiong et al., 2006). Unexpectedly, the secreted protease aureolysin was found to be a significant determinant of the *S. aureus* exoproteome. Inactivation of Sae leads to a significant increase in aureolysin abundance, consistent with previous reports demonstrating that aureolysin is repressed by Sae (Nygaard et al., 2010; Rogasch et al., 2006). Thus, in addition to transcriptional regulation by Sae, our results suggest an additional tier of regulation of the *S. aureus* virulence repertoire, whereby secreted protein abundance is tailored by the expression of a staphylococcal protease. These data corroborate findings from a previous study in which inactivation of all extracellular proteases led to changes in the *S. aureus* proteome (Zielinska et al., 2012). The benefit of such posttranslational processing of virulence factors is unknown, but it is possible that this strategy allows *S. aureus* to combat the innate immune system while limiting antigenic accessibility to the adaptive immune response. An alternative explanation is that aureolysin-mediated processing of the secreted virulence repertoire allows *S. aureus* to modulate virulence factor production in response to host microenvironments. Staphylococcal abscesses are largely devoid of zinc, and thus a zinc-dependent protease such as aureolysin might allow for tailoring of the *S. aureus* secretome according to nutrient availability (Corbin et al., 2008). Aureolysin activity is also dependent on calcium, and therefore fluctuation of calcium availability at infectious foci may also modulate the secreted virulence repertoire (Arvidson, 1973). Finally, posttranslational regulation of secreted proteins by aureolysin might be a mechanism to govern the temporal and spatial abundance of specific toxins, allowing for more rapid changes in protein turnover and localization than can be achieved through transcriptional regulation alone.

The alpha-type PSMs were identified as osteolytic peptides that incite osteoblast cell death and contribute to pathogen-induced bone destruction during osteomyelitis. These results

Table 2. Select Proteins Altered in Abundance upon Concomitant Inactivation of *sae* and *aur*

Proteins[a]	Mean LAC Spectra	Mean LACΔ*sae*/*aur* Spectra	LAC/ LACΔ*saeaur*[b]	Quasi p Value[c]	Description
Significantly Decreased: Toxins, Proteases, and Exoenzymes					
Q2FHS2|Q2FHS2_STAA3	242.3333	0.6667	363.5000	0.0004	Alpha-hemolysin; SAUSA300_1058
Q2FFA3|LUKL1_STAA3	152.6667	2.6667	57.2500	0.0048	LukA; SAUSA300_1974
Q2FE78|Q2FE78_STAA3	53.6667	1.0000	53.6667	0.0040	Gamma-hemolysin component A; HlgA
Q2FFA2|LUKL2_STAA3	157.6667	4.3333	36.3846	0.0112	LukB; SAUSA300_1975
Q2FFS9|SPLA_STAA3	57.6667	2.3333	24.7143	0.0096	Serine protease SplA
Q2FFT1|SPLC_STAA3	24.3333	1.0000	24.3333	0.0101	Serine protease SplC
Q2FFT0|SPLB_STAA3	261.6667	12.0000	21.8056	0.0040	Serine protease SplB
Q2FFT3|SPLE_STAA3	93.6667	4.3333	21.6154	0.0026	Serine protease SplE
Q2FK40|Q2FK40_STAA3	19.3333	1.0000	19.3333	0.0133	Staphylocoagulase; Coa
Q2FFT4|SPLF_STAA3	75.3333	4.0000	18.8333	0.0046	Serine protease SplF
Q2FIK5|Q2FIK5_STAA3	12.0000	0.6667	18.0000	0.0208	Putative staphylocoagulase; SAUSA300_0773
Q2FFT2|SPLD_STAA3	71.0000	4.3333	16.3846	0.0049	Serine protease SplD
Q2FJL8|Q2FJL8_STAA3	4.6667	0.3333	14.0000	0.0352	Exotoxin 7; Set7
Q2FJP4|Q2FJP4_STAA3	58.6667	5.6667	10.3529	0.0040	Putative staphylococcal enterotoxin; SAUSA300_0370
Q2FGU9|Q2FGU9_STAA3	191.0000	20.3333	9.3934	0.0026	Panton-Valentine leukocidin, LukS-PV
Q2FKN2|RLMH_STAA3	3.0000	0.3333	9.0000	0.0454	Exotoxin; SAUSA300_0398
Q2FGV0|Q2FGV0_STAA3	600.0000	88.6667	6.7669	0.0049	Panton-Valentine leukocidin, LukF-PV
Q2FE77|Q2FE77_STAA3	19.0000	3.3333	5.7000	0.0125	Gamma-hemolysin component C; HlgC
Q2FIK2|Q2FIK2_STAA3	216.6667	43.0000	5.0388	0.0016	Thermonuclease; Nuc
Q2FJL3|Q2FJL3_STAA3	3.3333	0.6667	5.0000	0.0269	Exotoxin; SAUSA300_0401
Q2FJL6|Q2FJL6_STAA3	6.0000	1.3333	4.5000	0.0425	Exotoxin; SAUSA300_0398
Q2FJV7|Q2FJV7_STAA3	67.0000	20.3333	3.2951	0.0173	5′-nucleotidase, lipoprotein e(P4) family; SAUSA300_0307
Q2FFR8|Q2FFR8_STAA3	26.6667	8.3333	3.2000	0.0133	Leukotoxin LukE
Q2FHS0|Q2FHS0_STAA3	6.3333	2.0000	3.1667	0.0387	Putative exotoxin 4; SAUSA300_1060
Q2FJL9|Q2FJL9_STAA3	3.0000	0.0000	3.0000	0.0127	Exotoxin; SAUSA300_0395
Q2FE76|Q2FE76_STAA3	74.6667	28.0000	2.6667	0.0381	Gamma-hemolysin component B; HlgB
Q2FFR9|Q2FFR9_STAA3	55.3333	29.6667	1.8652	0.0251	Leukotoxin LukD
Q2FJU4|Q2FJU4_STAA3	6.3333	3.6667	1.7273	0.0454	Triacylglycerol lipase; SAUSA300_0320
Q2FKN3|Q2FKN3_STAA3	39.3333	34.3333	1.1456	0.0154	5′-nucleotidase family protein; SAUSA300_0025
Significantly Decreased: Immunomodulatory					
Q2FFF7|CHIPS_STAA3	856.0000	6.6667	128.4000	0.0016	Chemotaxis inhibitory protein; Chp
Q2FE79|SBI_STAA3	85.6667	1.6667	51.4000	0.0070	Immunoglobulin-binding protein Sbi
Q2FHS7|FLIPR_STAA3	10.0000	1.0000	10.0000	0.0091	FPRL1 inhibitory protein; Flr
Significantly Decreased: Regulatory					
Q2FKE7|Q2FKE7_STAA3	2.3333	0.6667	3.5000	0.0329	Staphylococcal accessory regulator SarS; SAUSA300_0114
Significantly Decreased: Surface/Cell-Wall Associated					
Q2FE03|FNBA_STAA3	19.3333	1.0000	19.3333	0.0131	Fibronectin-binding protein A; FnbA
Q2FHS5|Q2FHS5_STAA3	31.3333	2.6667	11.7500	0.0040	Fibrinogen-binding protein; Efb
Q2FE04|Q2FE04_STAA3	4.0000	0.6667	6.0000	0.0179	Fibronectin-binding protein B; FnbB
Q2FG07|ISDH_STAA3	20.0000	14.3333	1.3953	0.0454	Iron-regulated surface determinant protein H; IsdH
Q2FHV2|ISDB_STAA3	36.6667	27.0000	1.3580	0.0199	Iron-regulated surface determinant protein B; IsdB
Significantly Increased: Toxins, Proteases, and Exoenzymes					
Q2FG30|Y1654_STAA3	0.6667	12.3333	0.0541	0.0101	Uncharacterized peptidase SAUSA300_1654; SAUSA300_1654
Q2FHF9|Q2FHF9_STAA3	0.6667	10.6667	0.0625	0.0393	Peptidase, M16 family; SAUSA300_1172
Q2FJD0|Q2FJD0_STAA3	0.6667	8.6667	0.7693	0.0302	ATP-dependent zinc metalloprotease FtsH
Q2FIM5|CLPP_STAA3	1.6667	12.6667	0.1316	0.0189	ATP-dependent Clp protease proteolytic subunit; ClpP

(*Continued on next page*)

Table 2. *Continued*

Proteins[a]	Mean LAC Spectra	Mean LACΔ*sae/aur* Spectra	LAC/ LACΔ*saeaur*[b]	Quasi p Value[c]	Description
Q2FJB5|CLPC_STAA3	4.3333	25.0000	0.1733	0.0339	ATP-dependent Clp protease ATP-binding subunit ClpC
Q2FG62|CLPX_STAA3	0.0000	3.3333	0.3000	0.0173	ATP-dependent Clp protease ATP-binding subunit ClpX
Significantly Increased: Regulatory					
Q2FG02|Q2FG02_STAA3	1.3333	25.0000	0.0533	0.0389	Catabolite control protein A; CcpA
Q2FF85|Q2FF85_STAA3	0.6667	7.0000	0.0952	0.0497	Accessory gene regulator protein A; AgrA
Q2FIV3|Q2FIV3_STAA3	4.3333	33.0000	0.1313	0.0145	Transcriptional regulator, MarR family; SAUSA300_0672
Q2FJ20|SARA_STAA3	11.3333	64.6667	0.1752	0.0040	Transcriptional regulator SarA
Q2FF59|RSBW_STAA3	2.0000	8.6667	0.2308	0.0097	Serine-protein kinase RsbW
Q2FH23|ARLR_STAA3	0.0000	3.3333	0.3000	0.0173	Response regulator ArlR
Significantly Increased: Surface/Cell-Wall Associated					
Q2FKM6|Q2FKM6_STAA3	49.6667	239.6667	0.2072	0.0496	Penicillin-binding protein 2′; MecA
Q2FGW1|EBPS_STAA3	5.6667	20.0000	0.2833	0.0417	Elastin-binding protein EbpS

See also Table S2 for a complete list of proteins that change in abundance upon concomitant inactivation of *sae* and *aur.*

[a]UniprotKB nomenclature (http://www.uniprot.org).

[b]Ratio of mean LAC spectra divided by mean LACΔ*sae/aur* spectra. If mean spectra equaled zero, a value of one was used to calculate ratio. Values greater than 1.0 indicate protein abundances decreased upon inactivation of *sae* and *aur*. Values less than 1.0 indicate protein abundances increased upon inactivation of *sae* and *aur*.

[c]False-discovery-rate-corrected p value as calculated by the QuasiTel program.

confirm that aureolysin-mediated processing of secreted virulence factors shapes the staphylococcal virulence repertoire. As aureolysin is known to activate other extracellular proteases, it is possible that PSMs are also degraded by a second, aureolysin-activated secreted protease in the absence of Sae (Nickerson et al., 2007). However, previous studies demonstrated that aureolysin is capable of degrading PSMs in the absence of the *S. aureus* global regulator, SarA (Zielinska et al., 2011). PSM production is also dependent on an intact *agr* locus, and therefore the decreased cortical bone destruction observed in Δ*agr*-infected femurs may be a reflection of the absence of PSMs (Wang et al., 2007). Interestingly, as USA300 lineage strains of *S. aureus* are characterized by enhanced production of PSMs relative to other *S. aureus* clinical strain lineages (Li et al., 2009), our results may partially explain the increased morbidity associated with USA300 strains in patients with osteomyelitis (Carrillo-Marquez et al., 2009; Gonzalez et al., 2006).

Inactivation of aureolysin in the Δ*sae* background did not fully restore bone destruction to wild-type levels or significantly impact intraosseous bacterial survival. Similarly, inactivation of the alpha-type PSMs failed to affect pathogenesis to the same extent as inactivation of *sae*. It is therefore likely that additional Sae-regulated factors that impact the pathogenesis of osteomyelitis are yet to be discovered. Exoproteome analyses revealed that Sae affects the abundance of several classes of virulence factors, including factors that combat the innate immune system, cytotoxins, and degradative exoenzymes. In addition to secreted virulence factors, inactivation of Sae significantly decreased the abundance of cell surface proteins such as fibronectin- and fibrinogen-binding proteins. Therefore, the virulence defect of Δ*sae* may also reflect deficiencies in host-tissue binding, biofilm formation, or invasion of host cells. By defining the Sae exoproteome and aureolysin-mediated processing of secreted virulence factors, this work provides a foundation for the development of immunotherapeutics that limit pathologic bone remodeling during osteomyelitis, thereby enhancing the ability to treat staphylococcal musculoskeletal infection.

EXPERIMENTAL PROCEDURES

Ethics Statement

All experiments involving animals were reviewed and approved by the Institutional Animal Care and Use Committee of Vanderbilt University. All experiments were performed according to NIH guidelines, the Animal Welfare Act, and US Federal law.

Bacterial Strains and Growth Conditions

All experiments were conducted with derivatives of the USA300 type *S. aureus* clinical isolate LAC (WT). Bacterial strains were routinely grown on tryptic soy broth (TSB) solidified with 1.5% agar at 37°C or in TSB with shaking at 180 rpm, unless otherwise indicated. TSB was supplemented with 10 μg/ml erythromycin where indicated. Erythromycin-sensitive LAC (AH1263), Δ*sae*, Δ*agr*, Δ*agr/sae*, FPR3757 Δ*sae/aur*, and Newman Δ*psmα1-4* were previously described (Beenken et al., 2010; Benson et al., 2012; Boles et al., 2010; Kaito et al., 2011; Mrak et al., 2012). Strain Δ*sae/aur* was created by bacteriophage phi-85-mediated transduction of the *aur::erm* mutation from FPR3757 Δ*sae/aur* into the LAC Δ*sae* background as previously described (Mazmanian et al., 2003). Strain Δ*psmα1-4* was created by bacteriophage phi-85-mediated transduction of the *psmα1-4::erm* mutation from Newman Δ*psmα1-4* into LAC. Successful transduction was confirmed by targeted PCR, hemolysis pattern, and exoprotein pattern (data not shown).

Murine Model of Osteomyelitis

Bacterial inocula were prepared by 1:100 subculture of overnight TSB cultures followed by growth at 37°C and 180 rpm shaking for 3 hr. Bacteria were collected by centrifugation, washed with PBS, and resuspended to a concentration of 1×10^6 cfu in 2 μl PBS. Prior to surgery, 7- to 8-week-old C57BL/6J mice received 0.1 mg/kg buprenorphine via subcutaneous injection. Anesthesia was accomplished with isoflurane. The left hindlimb was shaved and disinfected, and a small incision was made overlying the lateral aspect of the left femur. The femur was exposed with blunt dissection, and a 1 mm diameter unicortical bone defect was created at the midfemur by trephination with a 21-gauge PrecisionGlide needle (Becton Dickinson). Bacterial inocula (1×10^6 cfu in 2 μl) were delivered through the bone defect into the intramedullary canal. Muscle fasciae and skin were then closed with suture, and mice were

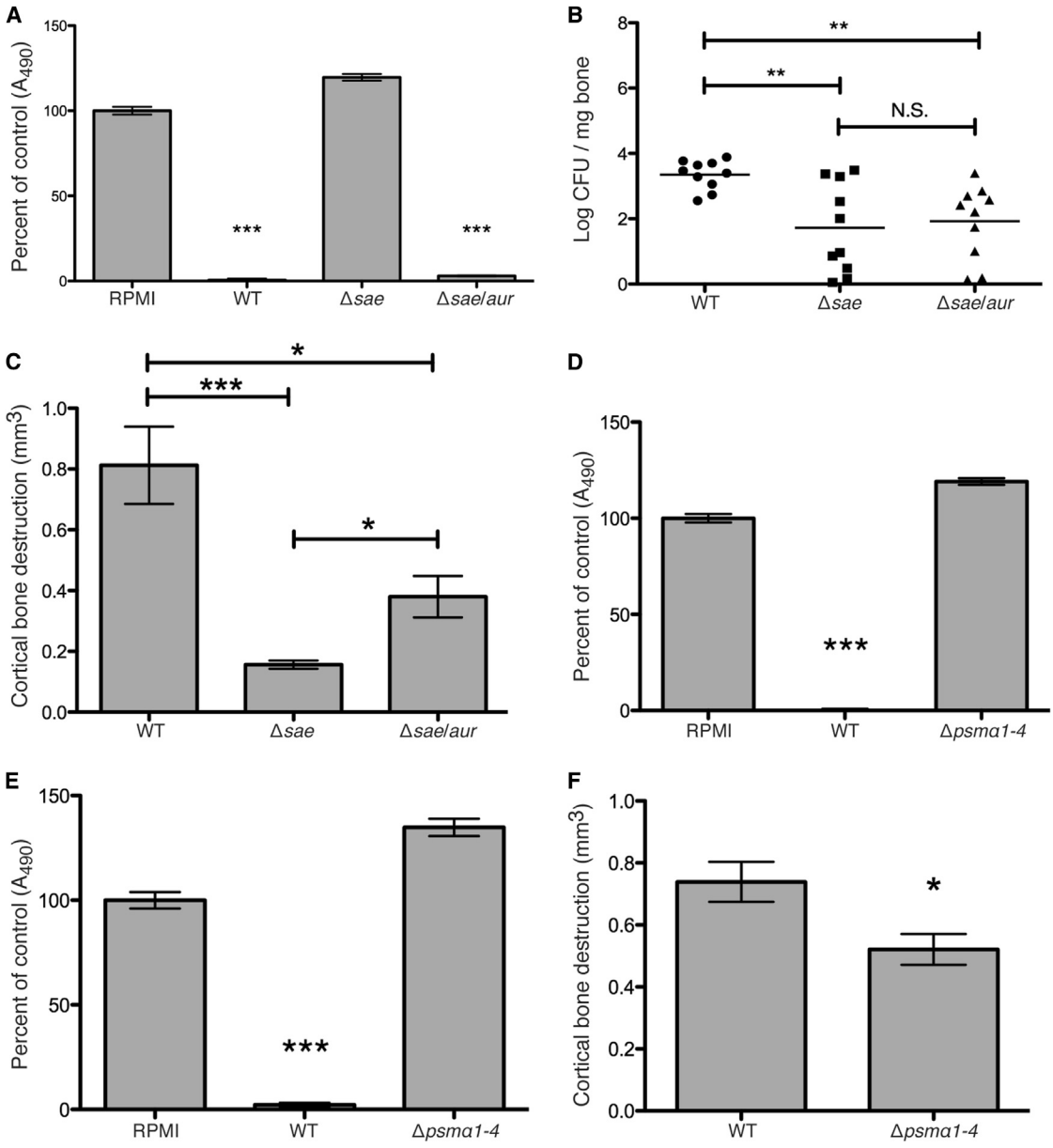

Figure 5. Alpha-Type Phenol-Soluble Modulins Are Aureolysin-Processed Peptides that Trigger Osteoblast Cell Death In Vitro and Contribute to Cortical Bone Destruction In Vivo

(A) MC3T3 cells (5,000 cells per well) were incubated with 40 μl concentrated culture supernatant from the indicated strains or an equivalent volume of sterile RPMI supplemented with 1% casamino acids (control). Osteoblast viability was assessed 23 hr later with the Promega CellTiter 96 AQueous One kit, and results are expressed as percent of control. n = 10 per group and results are representative of at least three independent experiments. Error bars indicate the SEM. ***$p < 0.001$ as calculated by a Student's t test.

(B and C) Groups of mice were subjected to experimental osteomyelitis via inoculation of WT, Δ*sae*, or Δ*sae/aur*. Femurs were harvested at 14 days post-inoculation and processed for bacterial recovery (n = 10 per group; B) or subjected to microCT imaging analysis of cortical bone destruction (n = 5 per group; C). Error bars indicate the SEM. *$p < 0.05$, **$p < 0.01$, and ***$p < 0.001$ as calculated by a Student's t test. Horizontal bars represent the mean of log cfu/mg of bone.

(D and E) MC3T3 (D) or Saos-2 (E) cell monolayers were incubated with 40 μl concentrated culture supernatant from the indicated strains or an equivalent volume of sterile RPMI supplemented with 1% casamino acids (control). Osteoblast viability was determined 23 hr later as above. Error bars indicate the SEM. ***$p < 0.001$ as calculated by a Student's t test.

(F) Groups of mice (n = 10 per group) were subjected to experimental osteomyelitis via inoculation of WT or Δ*psmα1-4*. Femurs were harvested at 14 days postinoculation and subjected to microCT imaging analysis of cortical bone destruction. Error bars indicate the SEM. *$p < 0.05$ relative to WT as calculated by a Student's t test.

See also Figure S3.

recovered from anesthesia. Buprenorphine was administered every 12 hr for 72 hr postoperatively, and then as needed thereafter. Infection was allowed to proceed for 14 days, at which time mice were euthanized and the left femur was removed and subjected to either microCT or processed for cfu enumeration. For cfu enumeration, femurs were separated from surrounding soft tissue, frozen in liquid nitrogen, and homogenized in a BioSpec Biopulverizer (Biospec Products). Homogenized bone was weighed and subsequently resuspended in 1 ml PBS prior to sonication in an ice water bath for 30 min. Sonicated homogenates were vortexed for 60 s and then serially diluted and plated on TSB solidified with 1.5% agar. Differences in cfu counts from groups of mice were analyzed with a Student's t test.

Microcomputed Tomography

Analysis of cortical bone destruction and new bone formation was determined by microCT imaging with a μCT50 (Scanco Medical) and the manufacturer's analytical software. Axial images of each femur were acquired with 5.0 μm voxels at 70 kV, 200 μA, 2,000 projections per rotation, and an integration time of 350 ms in a 10.24 mm field of view. Each imaging scan comprised 1,635 slices (8.125 mm) of the length of the femur, centered on the inoculation site as visualized in the scout-view radiographs. For analysis of cortical bone destruction, a volume of interest (VOI) including only the original cortical bone and any destruction was selected by drawing of inclusive contours on the periosteal surface and excluding contours on the endosteal surface. Volume of cortical bone destruction was determined by segmentation of the image with a lower threshold of 0 and an upper threshold of 595 mg HA/ccm, sigma 1.3, and support 1, to exclude bone in the analysis. For measurement of new bone volume, an inclusive contour was placed around the outer perimeter of the bone and an excluding contour was drawn along the preexisting periosteal surface. Bone was segmented from nonmineralized tissues in the VOI with a lower threshold of 400 mg HA/ccm, sigma 1.3, and support 2. The direct voxel counting method was used for all reported calculations in each analysis. Differences in cortical bone destruction and peripheral new bone formation were analyzed with a Student's t test.

Histopathology

After dissection, femurs were placed in neutral-buffered formalin. After 72 hr of formalin fixation at 4°C, samples were rinsed with deionized water and stored in 70% ethanol at 4°C. Femurs were subsequently decalcified in 20% EDTA (pH 7.4) at 4°C for 4 days. Decalcified samples were then dehydrated and embedded in paraffin. Serial 4 μm paraffin sections were taken with a Leica 2255RM microtome on Leica Superfrost glass slides. Paraffin sections were cleared with Histo-Clear, then dehydrated and stained with a modified H&E-phloxine-orange G stain. With this stain, bone tissue stains yellow to orange in color, osteoclasts stain a vibrant pink, mesenchymal cells stain blue, and bacterial biofilm stains pink to bright red.

Osteoblast Cytotoxicity Assays

MC3T3-E1 and Saos-2 cells were obtained from the American Type Culture Collection (ATCC) and propagated according to ATCC recommendations. Cells were grown at 37°C and 5% CO_2 with replacement of media every 2 or 3 days. For cytotoxicity assays, cells were seeded into 96-well tissue culture grade plates at a density of 2,500 or 5,000 cells per well for MC3T3 cells, or 10,000 cells per well for Saos-2 cells. After 24 hr, growth media was removed and replaced with media containing various amounts of concentrated *S. aureus* culture supernatant or an equivalent volume of sterile RPMI. For some experiments, varying amounts of unconcentrated, 0.22 μm filter-sterilized culture supernatant was added to cell monolayers. Monolayers were incubated for an additional 23 hr prior to replacement of growth media and assessment of cell viability with the CellTiter 96 AQueous One kit (Promega) per the manufacturer's instructions. So that the ability of alpha-type PSMs to induce osteoblast cytotoxicity could be tested, PSMα1, PSMα2, PSMα3, and PSMα4 were synthesized at >90% purity by AAPPTec. Purified peptides were resuspended in dimethyl sulfoxide and added at varying concentrations to osteoblast monolayers prior to assessment of cell viability as above. To test the impact of aureolysin activity on PSM cytotoxicity, purified aureolysin (Biocentrum) was incubated with PSMα2 and PSMα3 for 8 hr at 37°C at a ratio of 1 μg aureolysin per 2 μg PSM. Aureolysin-processed PSMs were then added to MC3T3 cell monolayers at 100 μg/ml final concentration, and cytotoxicity was assessed as above. As a control, aureolysin was heat inactivated for 30 min at 65°C prior to prior to incubation with PSMs and assessment of osteoblast cytotoxicity.

Preparation of Concentrated *S. aureus* Culture Supernatant

To prepare concentrated culture supernatant, a single bacterial colony was inoculated into 15 ml RPMI supplemented with 1% casamino acids in a 50 ml conical tube. Cultures were grown for 15 hr at 37°C and 180 rpm shaking, after which time they were normalized to an optical density 600 of 3.5 and subjected to centrifugation for supernatant collection. Triplicate culture supernatants were filtered through a 0.22 μm filter, combined, and concentrated with an Amicon Ultra 3 kDa nominal molecular weight limit centrifugal filter unit (Millipore) per the manufacturer's instructions. Supernatants were again filter sterilized and used immediately for cytotoxicity assays, proteomic analysis, or SDS-PAGE analysis. Supernatants were routinely plated onto tryptic soy agar supplemented with 5% sheep's blood for confirmation of sterility and hemolysis pattern. For SDS-PAGE analysis, 30 μl concentrated supernatant was resuspended in 4× loading buffer and boiled for 10 min. Proteins in the supernatant were resolved using 15% WT/vol SDS-PAGE and stained with Coomassie blue prior to digital imaging.

Proteomic Analysis of *S. aureus* Exoproteins

Concentrated culture supernatants were prepared from WT, Δ*sae*, and Δ*sae*/*aur* as outlined above. Supernatants were resuspended in LDS sample buffer (Life Technologies) prior to resolution of the proteins at approximately 1 cm with a 10% Novex precast gel. Resolved proteins were subjected to in-gel tryptic digestion to recover peptides. Recovered peptides were analyzed via MudPIT (Multidimensional Protein Identification Technology) per previously published protocols (MacCoss et al., 2002; Martinez et al., 2012). In brief, digested peptides were loaded onto a biphasic precolumn consisting of 4 cm of reversed phase (RP) material followed by 4 cm of strong cation exchange (RP) material. Once loaded, the column was placed in line with a 20 cm RP analytical column packed into a nanospray emitter tip directly coupled to a linear ion trap mass spectrometer (LTQ). A subset of peptides was eluted from the SCX material onto the RP analytical via a pulse of volatile salt, separated by an RP gradient, and then ionized directly into the mass spectrometer where both the intact masses (mass spectrometry) and fragmentation patterns (tandem mass spectrometry) of the peptides were collected. These peptide spectral data were searched against a protein database with Sequest (Yates et al., 1995), and the resulting identifications were collated and filtered with IDPicker (Ma et al., 2009) and Scaffold (Proteome Software). Relative protein abundances were evaluated via spectral counting techniques using the QuasiTel program to calculate false discovery rate-corrected p values (Li et al., 2010).

SUPPLEMENTAL INFORMATION

Supplemental Information includes three figures and two tables and can be found with this article online at http://dx.doi.org/10.1016/j.chom.2013.05.003.

ACKNOWLEDGMENTS

We thank Lorenzo Olive, Ian Marriott, Florent Elefteriou, and Jon Schoenecker for assistance with surgical procedures. We thank the Vanderbilt Mass Spectrometry Research Center Proteomics Laboratory for assistance with exoproteome determinations. We are thankful to Dr. Chikara Kaito (The University of Tokyo) for providing Newman Δ*psmα1-4*. This research was supported by National Institutes of Health grants S10RR027631-01 to D.S.P., AI073843 and AI069233 to E.P.S., T32HD060554-03 to J.E.C., and AI091856 to V.J.T. V.J.T. was also supported by funds from the American Heart Association (Scientist Development Grant 09SDG2060036) and New York University School of Medicine Development Funds. M.A.B. was supported in part by an American Heart Association predoctoral fellowship (10PRE3420022). E.P.S. is a Burroughs Wellcome Fellow in the Pathogenesis of Infectious Diseases.

Received: March 15, 2013
Revised: April 21, 2013
Accepted: April 30, 2013
Published: June 12, 2013

REFERENCES

Alexander, E.H., Rivera, F.A., Marriott, I., Anguita, J., Bost, K.L., and Hudson, M.C. (2003). *Staphylococcus aureus* - induced tumor necrosis factor - related apoptosis - inducing ligand expression mediates apoptosis and caspase-8 activation in infected osteoblasts. BMC Microbiol. *3*, 5.

Arvidson, S. (1973). Studies on extracellular proteolytic enzymes from *Staphylococcus aureus*. II. Isolation and characterization of an EDTA-sensitive protease. Biochim. Biophys. Acta *302*, 149–157.

Beenken, K.E., Mrak, L.N., Griffin, L.M., Zielinska, A.K., Shaw, L.N., Rice, K.C., Horswill, A.R., Bayles, K.W., and Smeltzer, M.S. (2010). Epistatic relationships between *sarA* and *agr* in *Staphylococcus aureus* biofilm formation. PLoS ONE *5*, e10790.

Belthur, M.V., Birchansky, S.B., Verdugo, A.A., Mason, E.O., Jr., Hulten, K.G., Kaplan, S.L., Smith, E.O., Phillips, W.A., and Weinberg, J. (2012). Pathologic fractures in children with acute *Staphylococcus aureus* osteomyelitis. J. Bone Joint Surg. Am. *94*, 34–42.

Benson, M.A., Lilo, S., Nygaard, T., Voyich, J.M., and Torres, V.J. (2012). Rot and SaeRS cooperate to activate expression of the staphylococcal superantigen-like exoproteins. J. Bacteriol. *194*, 4355–4365.

Boles, B.R., Thoendel, M., Roth, A.J., and Horswill, A.R. (2010). Identification of genes involved in polysaccharide-independent *Staphylococcus aureus* biofilm formation. PLoS ONE *5*, e10146.

Carrillo-Marquez, M.A., Hulten, K.G., Hammerman, W., Mason, E.O., and Kaplan, S.L. (2009). USA300 is the predominant genotype causing *Staphylococcus aureus* septic arthritis in children. Pediatr. Infect. Dis. J. *28*, 1076–1080.

Claro, T., Widaa, A., McDonnell, C., Foster, T.J., O'Brien, F.J., and Kerrigan, S.W. (2013). *Staphylococcus aureus* protein A binding to osteoblast tumour necrosis factor receptor 1 results in activation of nuclear factor kappa B and release of interleukin-6 in bone infection. Microbiology *159*, 147–154.

Corbin, B.D., Seeley, E.H., Raab, A., Feldmann, J., Miller, M.R., Torres, V.J., Anderson, K.L., Dattilo, B.M., Dunman, P.M., Gerads, R., et al. (2008). Metal chelation and inhibition of bacterial growth in tissue abscesses. Science *319*, 962–965.

Ellington, J.K., Reilly, S.S., Ramp, W.K., Smeltzer, M.S., Kellam, J.F., and Hudson, M.C. (1999). Mechanisms of *Staphylococcus aureus* invasion of cultured osteoblasts. Microb. Pathog. *26*, 317–323.

Gerber, J.S., Coffin, S.E., Smathers, S.A., and Zaoutis, T.E. (2009). Trends in the incidence of methicillin-resistant *Staphylococcus aureus* infection in children's hospitals in the United States. Clin. Infect. Dis. *49*, 65–71.

Goerke, C., Fluckiger, U., Steinhuber, A., Bisanzio, V., Ulrich, M., Bischoff, M., Patti, J.M., and Wolz, C. (2005). Role of *Staphylococcus aureus* global regulators *sae* and *sigmaB* in virulence gene expression during device-related infection. Infect. Immun. *73*, 3415–3421.

Gonzalez, B.E., Teruya, J., Mahoney, D.H., Jr., Hulten, K.G., Edwards, R., Lamberth, L.B., Hammerman, W.A., Mason, E.O., Jr., and Kaplan, S.L. (2006). Venous thrombosis associated with staphylococcal osteomyelitis in children. Pediatrics *117*, 1673–1679.

Gonzalez, D.J., Okumura, C.Y., Hollands, A., Kersten, R., Akong-Moore, K., Pence, M.A., Malone, C.L., Derieux, J., Moore, B.S., Horswill, A.R., et al. (2012). Novel phenol-soluble modulin derivatives in community-associated methicillin-resistant *Staphylococcus aureus* identified through imaging mass spectrometry. J. Biol. Chem. *287*, 13889–13898.

Hudson, M.C., Ramp, W.K., Nicholson, N.C., Williams, A.S., and Nousiainen, M.T. (1995). Internalization of *Staphylococcus aureus* by cultured osteoblasts. Microb. Pathog. *19*, 409–419.

Kaito, C., Saito, Y., Nagano, G., Ikuo, M., Omae, Y., Hanada, Y., Han, X., Kuwahara-Arai, K., Hishinuma, T., Baba, T., et al. (2011). Transcription and translation products of the cytolysin gene *psm-mec* on the mobile genetic element SCCmec regulate *Staphylococcus aureus* virulence. PLoS Pathog. *7*, e1001267.

Lew, D.P., and Waldvogel, F.A. (1997). Osteomyelitis. N. Engl. J. Med. *336*, 999–1007.

Lew, D.P., and Waldvogel, F.A. (2004). Osteomyelitis. Lancet *364*, 369–379.

Li, M., Diep, B.A., Villaruz, A.E., Braughton, K.R., Jiang, X., DeLeo, F.R., Chambers, H.F., Lu, Y., and Otto, M. (2009). Evolution of virulence in epidemic community-associated methicillin-resistant *Staphylococcus aureus*. Proc. Natl. Acad. Sci. USA *106*, 5883–5888.

Li, M., Gray, W., Zhang, H., Chung, C.H., Billheimer, D., Yarbrough, W.G., Liebler, D.C., Shyr, Y., and Slebos, R.J. (2010). Comparative shotgun proteomics using spectral count data and quasi-likelihood modeling. J. Proteome Res. *9*, 4295–4305.

Liang, X., Yu, C., Sun, J., Liu, H., Landwehr, C., Holmes, D., and Ji, Y. (2006). Inactivation of a two-component signal transduction system, SaeRS, eliminates adherence and attenuates virulence of *Staphylococcus aureus*. Infect. Immun. *74*, 4655–4665.

Ma, Z.Q., Dasari, S., Chambers, M.C., Litton, M.D., Sobecki, S.M., Zimmerman, L.J., Halvey, P.J., Schilling, B., Drake, P.M., Gibson, B.W., and Tabb, D.L. (2009). IDPicker 2.0: Improved protein assembly with high discrimination peptide identification filtering. J. Proteome Res. *8*, 3872–3881.

MacCoss, M.J., McDonald, W.H., Saraf, A., Sadygov, R., Clark, J.M., Tasto, J.J., Gould, K.L., Wolters, D., Washburn, M., Weiss, A., et al. (2002). Shotgun identification of protein modifications from protein complexes and lens tissue. Proc. Natl. Acad. Sci. USA *99*, 7900–7905.

Marriott, I., Gray, D.L., Tranguch, S.L., Fowler, V.G., Jr., Stryjewski, M., Scott Levin, L., Hudson, M.C., and Bost, K.L. (2004). Osteoblasts express the inflammatory cytokine interleukin-6 in a murine model of *Staphylococcus aureus* osteomyelitis and infected human bone tissue. Am. J. Pathol. *164*, 1399–1406.

Martinez, M.N., Emfinger, C.H., Overton, M., Hill, S., Ramaswamy, T.S., Cappel, D.A., Wu, K., Fazio, S., McDonald, W.H., Hachey, D.L., et al. (2012). Obesity and altered glucose metabolism impact HDL composition in CETP transgenic mice: a role for ovarian hormones. J. Lipid Res. *53*, 379–389.

Mazmanian, S.K., Skaar, E.P., Gaspar, A.H., Humayun, M., Gornicki, P., Jelenska, J., Joachmiak, A., Missiakas, D.M., and Schneewind, O. (2003). Passage of heme-iron across the envelope of *Staphylococcus aureus*. Science *299*, 906–909.

Mrak, L.N., Zielinska, A.K., Beenken, K.E., Mrak, I.N., Atwood, D.N., Griffin, L.M., Lee, C.Y., and Smeltzer, M.S. (2012). *saeRS* and *sarA* act synergistically to repress protease production and promote biofilm formation in *Staphylococcus aureus*. PLoS ONE *7*, e38453.

Nickerson, N.N., Prasad, L., Jacob, L., Delbaere, L.T., and McGavin, M.J. (2007). Activation of the SspA serine protease zymogen of *Staphylococcus aureus* proceeds through unique variations of a trypsinogen-like mechanism and is dependent on both autocatalytic and metalloprotease-specific processing. J. Biol. Chem. *282*, 34129–34138.

Nygaard, T.K., Pallister, K.B., Ruzevich, P., Griffith, S., Vuong, C., and Voyich, J.M. (2010). SaeR binds a consensus sequence within virulence gene promoters to advance USA300 pathogenesis. J. Infect. Dis. *201*, 241–254.

Peyrani, P., Allen, M., Seligson, D., Roberts, C., Chen, A., Haque, N., Zervos, M., Wiemken, T., Harting, J., Christensen, D., and Ramirez, R. (2012). Clinical outcomes of osteomyelitis patients infected with methicillin-resistant *Staphylococcus aureus* USA-300 strains. Am. J. Orthop. *41*, 117–122.

Rogasch, K., Rühmling, V., Pané-Farré, J., Höper, D., Weinberg, C., Fuchs, S., Schmudde, M., Bröker, B.M., Wolz, C., Hecker, M., and Engelmann, S. (2006). Influence of the two-component system SaeRS on global gene expression in two different *Staphylococcus aureus* strains. J. Bacteriol. *188*, 7742–7758.

Somayaji, S.N., Ritchie, S., Sahraei, M., Marriott, I., and Hudson, M.C. (2008). *Staphylococcus aureus* induces expression of receptor activator of NF-kappaB ligand and prostaglandin E2 in infected murine osteoblasts. Infect. Immun. *76*, 5120–5126.

Voyich, J.M., Vuong, C., DeWald, M., Nygaard, T.K., Kocianova, S., Griffith, S., Jones, J., Iverson, C., Sturdevant, D.E., Braughton, K.R., et al. (2009). The SaeR/S gene regulatory system is essential for innate immune evasion by *Staphylococcus aureus*. J. Infect. Dis. *199*, 1698–1706.

Wang, R., Braughton, K.R., Kretschmer, D., Bach, T.H., Queck, S.Y., Li, M., Kennedy, A.D., Dorward, D.W., Klebanoff, S.J., Peschel, A., et al. (2007).

Identification of novel cytolytic peptides as key virulence determinants for community-associated MRSA. Nat. Med. *13*, 1510–1514.

Weichert, S., Sharland, M., Clarke, N.M., and Faust, S.N. (2008). Acute haematogenous osteomyelitis in children: is there any evidence for how long we should treat? Curr. Opin. Infect. Dis. *21*, 258–262.

Xiong, Y.Q., Willard, J., Yeaman, M.R., Cheung, A.L., and Bayer, A.S. (2006). Regulation of *Staphylococcus aureus* alpha-toxin gene (*hla*) expression by *agr, sarA*, and *sae* in vitro and in experimental infective endocarditis. J. Infect. Dis. *194*, 1267–1275.

Yates, J.R., 3rd, Eng, J.K., McCormack, A.L., and Schieltz, D. (1995). Method to correlate tandem mass spectra of modified peptides to amino acid sequences in the protein database. Anal. Chem. *67*, 1426–1436.

Young, A.B., Cooley, I.D., Chauhan, V.S., and Marriott, I. (2011). Causative agents of osteomyelitis induce death domain-containing TNF-related apoptosis-inducing ligand receptor expression on osteoblasts. Bone *48*, 857–863.

Zielinska, A.K., Beenken, K.E., Joo, H.S., Mrak, L.N., Griffin, L.M., Luong, T.T., Lee, C.Y., Otto, M., Shaw, L.N., and Smeltzer, M.S. (2011). Defining the strain-dependent impact of the Staphylococcal accessory regulator (*sarA*) on the alpha-toxin phenotype of *Staphylococcus aureus*. J. Bacteriol. *193*, 2948–2958.

Zielinska, A.K., Beenken, K.E., Mrak, L.N., Spencer, H.J., Post, G.R., Skinner, R.A., Tackett, A.J., Horswill, A.R., and Smeltzer, M.S. (2012). *sarA*-mediated repression of protease production plays a key role in the pathogenesis of *Staphylococcus aureus* USA300 isolates. Mol. Microbiol. *86*, 1183–1196.